Long-Term Creep Data Prediction for Type 316H Stainless Steel

M.T. Whittaker, M. Evans and B. Wilshire

Materials Research Centre, College of Engineering, Swansea University, Swansea SA2 8PP, UK

Abstract

Impressive data sets have been produced for 316H stainless steel (18Cr-12Ni-Mo with up to 0.08C) by the National Institute for Materials Science (NIMS), Japan, to reveal the dependencies on stress and temperature of the high-temperature creep and creep fracture behaviour of nine batches of tube, six of bar and two of plate. Using these long-term property values, the stresses to produce failure in 100,000h at various plant exposure temperatures have been determined using the Manson-Haferd parameter. However, by incorporating the 0.2% proof stresses and ultimate tensile strengths of each batch of material at the creep temperatures, new relationships allow accurate prediction of the allowable tensile creep stresses using data from tests lasting only up to 5000h. Moreover, all of these results can be interpreted straightforwardly in terms of the dislocation processes controlling creep strain accumulation and the cavitation damage causing creep failure.

Keywords: Creep , Creep Fracture, Data Prediction, Austenitic Steels

1. Introduction

The selection of alloy steels for power plant service is usually based on the requirement that creep failure should not occur under the prevailing operating conditions during plant lives of ~250,000h (> 30 yrs). Although complex stresses and temperatures are often encountered, design decisions are generally made on the basis of the 'allowable tensile creep strengths' of the chosen materials. These strengths are commonly determined [1] as 67% of the average stress (up to 1088K) or 80% of the minimum stress causing creep rupture in 100,000h (~3.6×10^{8}s) or as the average stress producing a creep rate of 0.01%/1000h (~$3 \times 10^{-11} s^{-1}$).

Unfortunately, with the parametric, numerical and computational methods currently employed, 100,000h data cannot be predicted by extrapolation of short-term property measurements despite the international efforts being devoted to the different procedures available [2]. Hence, at present, protracted and expensive test programmes lasting 12-15 years are necessary to determine the required long-term estimates. A reduction in this 12-15 year 'materials development cycle' has therefore been defined as the No.1 priority in the 2007 UK Energy Materials – Strategic Research [3]. With the aim of reducing this 12-15 year cycle, over recent years, a new methodology has been devised which appears to allow 100,000h property values to be determined precisely by analysis of

short-term data [4-7], covering minimum creep rates ($\dot{\varepsilon}_m$), creep rupture lives (t_f) and times to various creep strains (t_ε). Specifically, using the Wilshire equations, 100,000h strength estimates have been derived accurately by analysis of multi-batch data sets obtained from tests lasting up to only 5000h for ferritic [7], bainitic [6] and martensitic steels [5]. This new approach quantifies t_f, $\dot{\varepsilon}_m$ and t_ε as functions of stress (σ) and temperature (T) as

$$(\sigma/\sigma_{TS}) = \exp\{-k_1 [t_f . \exp(-Q_c^*,/RT)]^u\} \quad (1)$$

$$(\sigma/\sigma_{TS}) = \exp\{-k_2 [\dot{\varepsilon}_m . \exp(Q_c^*RT)]^v\} \quad (2)$$

$$(\sigma/\sigma_{TS}) = \exp\{-k_3 [t_\varepsilon \exp(Q_c^*RT)]^w\} \quad (3)$$

where σ_{TS} is the ultimate tensile strength obtained from high-strain-rate (~$10^{-3}s^{-1}$) tensile tests carried out at the creep temperatures for each batch of material investigated. The various parameters, Q_c^*, k_1, k_2 and k_3, as well as u, v and w, are easily computed from t_f, $\dot{\varepsilon}_m$ and t_ε measurements made over reasonable stress/temperature ranges [4-7]. Since σ_{TS} is the highest possible stress which can be applied at the creep temperature, eqns (1), (2) and (3) then provide sigmoidal descriptions of the t_f, $\dot{\varepsilon}_m$ and t_ε values as systematically approaching t_f=0, t_ε =0 and $\dot{\varepsilon}_m$ = ∞ when $\sigma/\sigma_{TS}\rightarrow$ 1 and t_f=∞, t_ε = ∞ and $\dot{\varepsilon}_m$ = 0 as $\sigma/\sigma_{TS}\rightarrow$0.

Although the Wilshire equations have allowed accurate estimation of the 100,000h creep properties for various steels produced for constructions of power generation and petrochemical plant [5-7], as well as for pure copper [4] and aluminium alloys for airframe applications [8], for general applicability, the method must be validated for a wide range of other materials. For this reason, the present study considers type 316H stainless steel (18Cr-12Ni-Mo with up to 0.08% C). For this product, manufactured as tube [9], plate [10] and bar [11], reliable multi-batch $\dot{\varepsilon}_m$ and t_f properties have been determined over wide stress-temperature ranges by the National Institute for Materials Science (NIMS), Japan. Using these results, an assessment can be made of

(a) the accuracy with which the Wilshire equations predict measured 100,000h stress rupture values by analysis of data from tests lasting up to only 5000h, and

(b) how well the extrapolated 'allowable tensile creep strengths' estimated as 67% of the average stresses giving creep lives of from 100,000h compares with the predicted stresses giving minimum creep rates of 0.01%/1000h at the appropriate service temperatures.

In addition confidence in this new extrapolation procedure should be improved if the observed property sets can be discussed sensibly in terms of the processes of deformation and failure controlling creep and creep fracture behaviour.

2. Processing of Materials

The data sets produced by NIMS reported the 0.2% proof stresses (σ_{PS}) and ultimate tensile strengths (σ_{TS}), as well as the initial specimen extensions on loading (ε_0), the $\dot{\varepsilon}_m$, t_e and t_f values, the elongations to failure (ε_f) and the reductions in area at fracture (RoA) for nine batches of 316 tube at 873 to 1023K (600 to 750°C), for six batches of bar and two of plate at 873K to 1123K (600 to 850°C). These samples were labelled by NIMS as AAA to AAN for the tube [9], as ADA to ADF for the bar [11] and AaA to AaB for the plate [10]. In sets of three, the tube was heat treated as

(a) rotary pierced and cold drawn, followed by water quenching from 1373K (1100°C),

(b) hot extruded and cold drawn, followed by water quenching from 1403K (1130°C) and

(c) hot extruded and cold drawn followed by solution treatment [9]

For the bar, two of the six samples were processed after hot rolling [11] for

(i) 2h at 1353K (1080°C), before water quenching

(ii) 70 mins at 1373K (1100°C), then water quenched and

(iii) 110 mins at 1333K (1060°C) and water quenching.

The two plate specimens were hot rolled and held at 1323K (1050°C) for either 40 mins or 80 mins before water quenching [10].

3. Traditional Approaches to Creep and Creep Fracture

For well over half a century, the $\dot{\varepsilon}_m$ and t_f values been described using power law equations as

$$M/t_f = \dot{\varepsilon}_m = A\,\sigma^n \exp(-Q_c/RT) \qquad (4)$$

where $Q_c \neq Q_c$*) is the activation energy determined from the temperature dependence of $\dot{\varepsilon}_m$ and t_f at constant σ, not at constant (σ/σ_{TS}) as with eqns (1-3). With eqn (4), Q_c as well as the parameters (M and A) and the stress exponent (n) vary depending on the stress/temperature ranges considered. With all forms of the 316H samples studied, these variations are illustrated in Figs. 1 and 2, where the standard log σ/log $\dot{\varepsilon}_m$ and log σ/log t_f plots show that n decreases from 13 to about 4 with decreasing stress and increasing temperature, with Q_c varying from 270 to 730 kJmol^{-1}.

With the variations in n and Q_c evident from Figs. 1 and 2, power law relationships cannot be used to predict long-term properties from short-term results. Thus, to estimate the stresses giving creep lives of 100,000h [9-11], use was made of the Manson-Haferd parameter (P), namely [12],

$$P = \frac{\log t_f - \log t_a}{T - T_a} \qquad (5)$$

where T is in degrees Kelvin and t_f is the time to rupture (h), while t_a and T_a are optimized constants. The NIMS results obtained using eqn (5) are listed for tube, bar and plate in Table I [9-11], as illustrated for the bar samples in Fig 3.

4. New Creep Data Analyses

For the 316 tube, bar and plate, by applying eqn.(2), the best values of Q_c*, k_2 and v were determined as follows. Firstly, for each batch of material, Q_c* was estimated by superimposing the data sets at each creep temperature onto the least-squares straight lines. Essentially, superimposing the [$\dot{\varepsilon}_m$ exp (Q_c*/RT)] against ln[-ln (σ/σ_{TS})] plots showed two distinct lines for each batch, with Q_c* decreasing as the stress was reduced from above to below σ_{PS} (Fig.4). Because the composition and microstructure were comparable, despite slight differences in the Q_c* estimates, it was then assumed that Q_c* would be identical for $\sigma>\sigma_{PS}$, with a different value of Q_c* for $\sigma<\sigma_{PS}$. Hence, the derived Q_c*values were averaged to give Q_c*=250kJmol^{-1} for $\sigma>\sigma_{PS}$ and Q_c*=150kJmol^{-1} for $\sigma<\sigma_{PS}$. With Q_c* established from the ln [$\dot{\varepsilon}_m$ exp (Q_c*/RT)] against ln[-ln (σ/σ_{TS})] plots, the best values of k_2 and v were obtained for $\sigma>\sigma_Y$ and for $\sigma<\sigma_Y$ by averaging the results obtained over the stress ranges covered for the tube, bar and plate products, as listed in Table II.

From the results in Table II for each σ/σ_{TS} range, using eqn.(2), standard log σ/log $\dot{\varepsilon}_m$ plots were constructed, with the calculated lines in Fig.1 matching the measured NIMS properties. On this basis, the computed stresses to give creep rates of 0.01%/1000h (~3x10^{-11}s^{-1}) are listed in Table III, with these estimates based on $\dot{\varepsilon}_m$ values from tests with measured creep lives of less than 5000h.

The breaks in the lines shown in Fig.4, as previously reported for polycrystalline copper [4], occur at $\sigma=\sigma_Y$, where σ_Y is the yield stress for each batch determined from high-strain-rate tensile tests carried out at each creep temperature. For the 316H samples, $\sigma_Y \approx \sigma_{PS}$, indicating that the detailed processes controlling creep change when the applied stress is reduced from above to below this value. Thus, for $\sigma<\sigma_Y$ ($<\sigma_{PS}$), the initial strain on loading at the creep temperature (ε_0) increases elastically with increasing stress, but then increases more rapidly when plastic components of ε_0 occur when $\sigma>\sigma_Y$ ($>\sigma_{PS}$) (Fig.5).Clearly, when $\sigma>\sigma_Y$, dislocations are generated within the grains during the plastic component of ε_0, so creep is controlled by these newly created dislocations, with Q_c*=250 kJmol^{-1} being the activation energy for lattice diffusion within the austenitic grains. In contrast, when $\sigma<\sigma_Y$, new dislocations are not created within the grains, so creep must occur by movement of pre-existing dislocations not within the grains but in the grain boundary zones (i.e. by grain boundary sliding and associated dislocation movement in regions adjacent to grain boundaries). Consequently, when $\sigma<\sigma_Y$ ($<\sigma_{PS}$), Q_c*=150 kJmol^{-1} which coincides with the activation

energy for diffusion along grain boundaries and related dislocations near to the grain boundaries. Thus, the measured $\dot{\varepsilon}_m$ values when $\sigma<\sigma_Y$ are smaller than the figures predicted by linear extrapolation of the minimum creep rates recorded when $\sigma>\sigma_Y$ ($>\sigma_{PS}$).

5. New Creep Life Analyses

As shown in eqn. (4), the creep life depends on the minimum creep rate but, as demonstrated in Fig.6, the M value ($=\dot{\varepsilon}_m t_f$) decreases from around 0.01 towards about 0.001 or less as the creep life increases from approximately 3.6 x 10^5 to 3.6 x 10^8s. So, as with the representation of minimum creep rate data, using eqn.(2), the creep lives would also be expected to be well represented by eqn (1). In fact, as illustrated previously for $\dot{\varepsilon}_s$ in Fig.4, the results obtained by plotting ln [t_f exp (-Q_c*/RT)] against [-ln (σ/σ_{TS})] for type 316 stainless steel tube samples are well represented by two straight lines (Fig.7). Moreover, using computational procedures identical to those adopted to determine Q_c*, k_2 and v in eqn.(2), the best-fit values of Q_c*, k_1 and u are presented in Table IV for the type 316 tube, bar and plate. Using these figures to construct standard log σ/log t_f graphs, the calculated lines in Fig.2 closely match the measured NIMS t_f values.

By analysing t_f measurements for creep lives less than 5000h, the 100,000h rupture stresses were calculated using eqn (1). These figures are listed for 316H tube, bar and plate in Table V, clearly matching the 100,000h creep rupture stress estimates obtained by NIMS by applying the Manson-Haferd method (eqn (5)) to t_f values up to 100,000h (Table I). However, the average stresses required to give creep lives of 100,000h using the Manson-Haferd equation (Table I) and eqn.(1) (Table V) are substantially larger than the stresses to give creep rates of 3 x $10^{-11}s^{-1}$ (Table III). Even so, the stresses to give creep rates of 3 x $10^{-11}s^{-1}$ (Table III) are close to the 'allowable tensile creep strengths' calculated as 67% of the average stress causing creep rupture in 100,000h at different exposure temperatures (Tables I & II), as specified in the 2004 ASME Boiler and Pressure Vessel Code [1].

6. Deformation and Damage Processes

In an earlier study of the effects of prestraining in creep and creep fracture of 316 stainless steels [13], normal creep curves were recorded, as shown in Fig. 8. This form of curve has usually been considered, after the instantaneous strain on loading (ε_0), as showing a primary curve with a creep rate which decays continuously until a secondary or steady state period is reached, after which the creep rate accelerates again in the tertiary stage which terminates in fracture. However, plotting

these curves to show the variations in instantaneous creep rate ($\dot{\varepsilon}$) with increasing time (t) demonstrates that, rather than a secondary stage, only a minimum rate is found when the decaying primary rate is offset by the tertiary acceleration. On this basis, instead of seeking to clarify the mechanism governing secondary or 'steady state' creep, the property sets should be interpreted in relation to the processes controlling creep strain accumulation and the damage phenomena causing the tertiary acceleration and fracture.

In line with the conclusions drawn from other recent programmes [14], the present work suggests that dislocation processes are rate controlling, with no transition to diffusional mechanisms in low stress tests. However, a change in the dominant dislocation process occurs when σ falls from above to below σ_Y ($\cong \sigma_{PS}$). Thus, when $\sigma > \sigma_Y$, creep is controlled by the movement of dislocations newly generated during the plastic component of ε_0, whereas the creep rate is determined only by grain boundary zone deformation when $\sigma < \sigma_Y$, because no new dislocations are created during the elastic initial loading strain.

In relation to these deformation processes, tertiary creep and fracture are caused by the nucleation, growth and link-up of cavities formed mainly on grain boundaries approximately normal to the tensile stress axis. Indeed, metallographic studies [9-11] have verified that failure occurs by cavitation, seemingly with the incidence of cavity formation increasing with increasing test temperature and decreasing applied stress. Moreover, $\varepsilon_f \cong$ RoA (Fig. 9), indicating the virtual absence of neck formation.

It is commonly accepted that creep cavities are strain nucleated and, irrespective of the precise mechanisms favoured to account for cavity growth, the dependence of t_f on $\dot{\varepsilon}_m$ (Fig. 10) demonstrates that the rates of cavity development and the times to eventual failure are governed by the rates of creep strain accumulation. It is then suggested [14] that, because cavity development is strain controlled, the creep life is determined principally by boundary zone deformation. Assuming that a comparable level of grain boundary zone deformation is necessary to cause failure, the contribution of grain deformation to the overall creep rate decreases with increasing temperature and decreasing stress, accounting for the decrease in ε_f, as well as $\dot{\varepsilon}_m t_f$ and RoA, as σ falls below σ_Y ($\cong \sigma_{PS}$) in Fig 11.

7. Conclusions

The $\dot{\varepsilon}_m$ and t_f values determined by NIMS, Japan, for nine batches of type 316 stainless steel tube, six of bar and two of plate have been analysed using the Wilshire equations, namely,

$$\frac{\sigma}{\sigma_{TS}} = \exp\left\{-k_1\left[t_f \exp\left(\frac{-Q_c^*}{RT}\right)\right]^u\right\}$$ and

$$\frac{\sigma}{\sigma_{TS}} = \exp\left\{-k_2\left[\dot{\varepsilon}_m \exp\left(\frac{Q_c^*}{RT}\right)\right]^v\right\}$$

where σ_{TS} is the ultimate tensile strength at the creep temperature for each batch of material studied. Using these relationships, the stress to cause failure in 100,000h obtained by extrapolation of data from tests lasting only up to 5000h coincide well with the estimates derived by applying the Manson-Haferd parameter to very long term property values. Moreover, the allowable tensile creep strengths calculated as 67% of the average stress causing fracture in 100,000h are close to the stresses giving creep rates of 0.01%/1000h, as required by the 2004 ASME Boiler and Pressure Vessel Code [1].

When the normal creep curves recorded for type 316H stainless steel are plotted to show the variations in creep rate ($\dot{\varepsilon}$) with time, minimum rather than 'steady state' creep rates are always observed, where the decaying primary curves are offset by the tertiary accelerations. On this basis, instead of traditional procedures which seek to clarify the mechanisms controlling 'secondary' or 'steady state' creep, property sets should be interpreted in relation to the processes governing creep strain accumulation and the phenomena causing the tertiary acceleration and eventual failure.

The processes responsible for creep change at stresses above and below σ_Y ($\cong \sigma_{PS}$), where σ_Y is the yield stress and σ_{PS} is the 0.2% proof stress of each batch of material at the creep temperature. When $\sigma > \sigma_Y$, creep occurs by movement of new dislocations generated during the plastic component of the initial strain on loading (ε_0), whereas creep takes place by grain boundary zone deformation when fully elastic ε_0 values only are recorded when $\sigma < \sigma_Y$. Moreover, under all stress/temperature conditions, failure occurs by cavitation. Even so, the contribution of grain deformation to the overall creep rate decreases with decreasing stress and increasing temperature, leading to substantial decreases in $\dot{\varepsilon}_m t_f$, ε_f and ROA when σ falls below σ_Y.

References

1. Boiler and pressure vessel code', 2004, New York, ASME
2. Holdsworth SR. In Shibli IA, Holdsworth SR, Merckling G, editors. Creep and fracture of high temperature components – design and life assessment issues. London: DEStech Publ: 2005. P380.

3. Allen D, Garwood S. Energy materials – strategic research agenda. Materials Energy Review. IOMMM: 2007.
4. Wilshire B. Battenbrough A. Mater. Sci. Eng. A 2007; **443A**: 156.
5. Wilshire B. Scharning PJ. Int. Mater. Rev. 2008; **53**: 91.
6. Wilshire B. Scharning PJ. Mater. Sci. Tech. 2008; **24**: 1.
7. Wilshire B. Scharning PJ. Int. J. Press. Vessels Piping 2008; **85**: 739.
8. Wilshire B. Scharning PJ. J. Mater. Sci. 2008; **43**: 3992.
9. NIMS Creep Data Sheet no.6B. Data Sheets on the Elevated-Temperature Properties of 18Cr-12Ni-Mo Stainless Steel Tubes for Boilers and Heat Exchangers (316H).
10. NIMS Creep Data Sheet no.14B. Data Sheets on the Elevated-Temperature Properties of 18Cr-12Ni-Mo Stainless Steel Plates for Reactor Vessels (316HP).
11. NIMS Creep Data Sheet no.15B. Data Sheets on the Elevated-Temperature Properties of 18Cr-12Ni-Mo Stainless Steel Bars for General Applications (316H).
12. S.S. Manson and A.M. Haferd: NASA TN2890, 1953.
13. Wilshire B. Willis M. Metal. Mater. Trans. A. 2004; **35A**: 563.
14. Wilshire B. Whittaker MT. Acta Mater. 2009; **57**: 4115.

Captions

Table I. The average stresses calculated to give creep lives of 100,000h for tube, bar and plate samples of 316H stainless steel at 873 to 1123K. These stresses were determined by applying the Manson-Haferd equation [12] to long-term NIMS data [9-11].

	Tube	Plate	Bar
873	120.0	136.5	106.5
923	65.9	65.5	54.8
973	36.4	38	32.2
1023	22.9	22.5	19.5
1073	18.6	17	13.5
1123	15.5	14.5	10

Table II. The average values of Q_c*, k_2 and v calculated by applying eqn.(2) to the minimum creep rates determined at stresses above and below σ_{PS} for the tube, bar and plate samples of 316H stainless steel.

	Tube		Plate		Bar	
	$\sigma>\sigma_{PS}$	$\sigma<\sigma_{PS}$	$\sigma>\sigma_{PS}$	$\sigma<\sigma_{PS}$	$\sigma>\sigma_{PS}$	$\sigma<\sigma_{PS}$
Q_c* (kJmol^{-1})	250	150	250	150	250	150
v	0.081	-0.053	-	-0.112	-	-0.112
k_2	4.48	1.63	-	2.35	-	2.35

Table III. Using eqn.(2) together with the data listed in Table II, the average stresses giving minimum creep rates of 3 x $10^{-11}s^{-1}$ are listed at 873 to 1123K for the tube, bar and plate samples of 316H stainless steel. These values were calculated by analysing minimum creep rate properties from tests with total creep lives less than 5000h.

	Tube	Plate	Bar
873K	110	50.7	55.2
923K	68.5	33.8	37.5
973K	53.7	20.8	24.1
1023K	39.8	12.9	15.5
1073K	-	7.6	9.5
1123K	-	4.6	6.1

Table IV. The average values of Q_c*, k_1 and u calculated by applying eqn.(1) to the creep lives determined at stresses above and below σ_{PS} for tube, bar and plate samples of 316H stainless steel.

	Tube		Plate		Bar	
	$\sigma>\sigma_{PS}$	$\sigma<\sigma_{PS}$	$\sigma>\sigma_{PS}$	$\sigma<\sigma_{PS}$	$\sigma>\sigma_{PS}$	$\sigma<\sigma_{PS}$
Q_c* (kJmol^{-1})	250	150	250	150	250	150
u	0.158	0.116	0.171	0.143	0.174	0.133
k_1	13.28	1.66	15.6	1.87	17.65	1.84

Table V. The average stresses calculated to give creep rupture lives of 100,000h at 873 to 1123K for tube, bar and plate samples of 316H stainless steel. These values were obtained using eqn.(1), plus the data in Table IV, to analyse creep life properties from tests with times to failure less than 5000h.

	Tube	Plate	Bar
873K	116.3	118.6	109.2
923K	63.7	65.5	56.6

973K	46.2	30.2	34.8
1023K	28.5	19.7	21.7
1073K	-	11.3	12.8
1123K	-	6.6	7.9

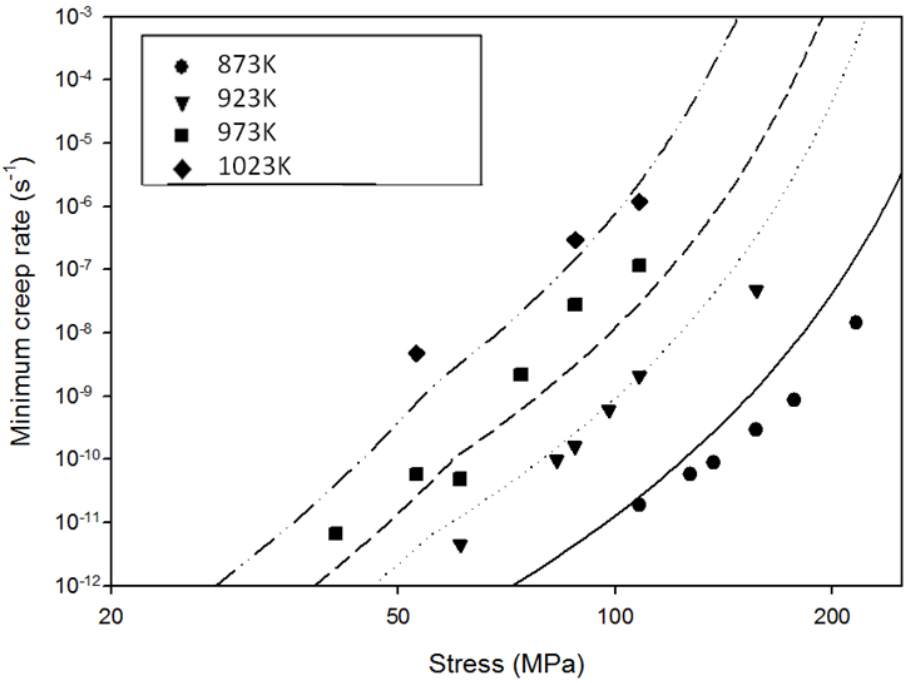

Figure 1. The variations of the minimum creep rate with stress expressed using eqn.(4), together with the lines calculated from eqn.(2) and the data in Table II for type 316H stainless steel tube.

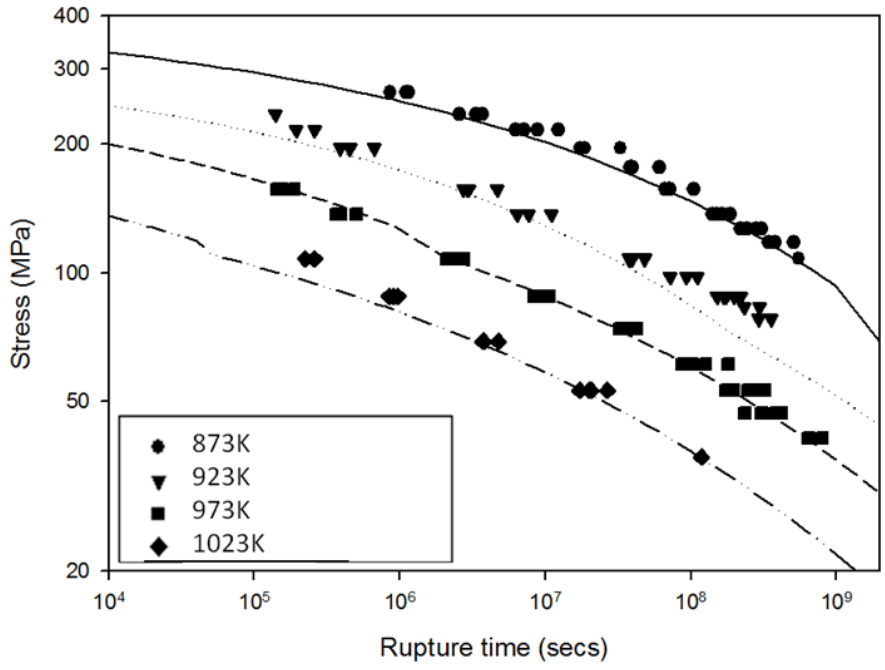

Figure 2. The variations in creep life with stress expressed using eqn.(4), together with the lines calculated from eqn.(1) and the data in Table IV for type 316H stainless steel tube.

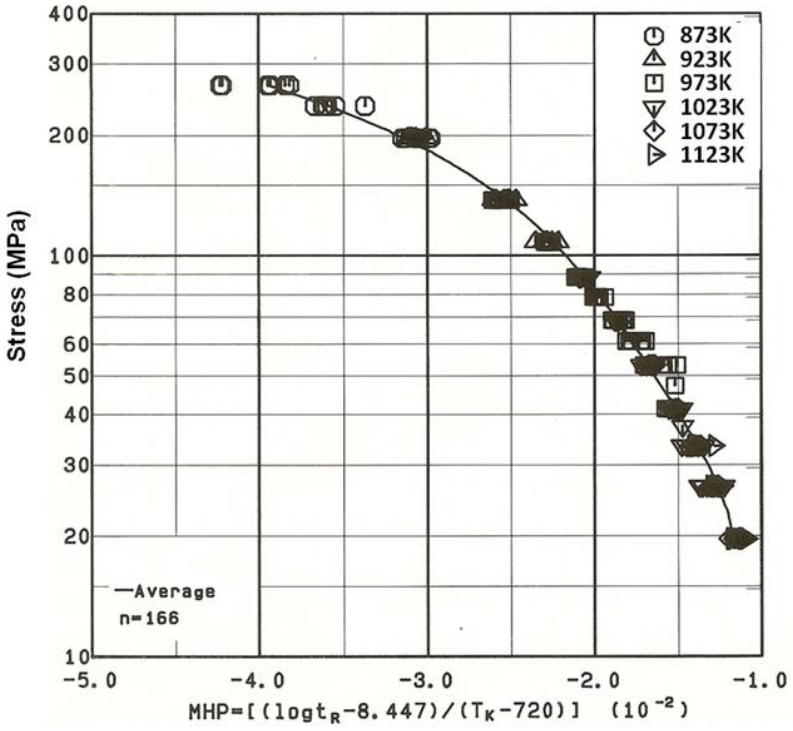

Figure 3. Plot showing the application of the application of the Manson-Haferd equation to creep rupture data obtained for samples of type 316H stainless steel bar.

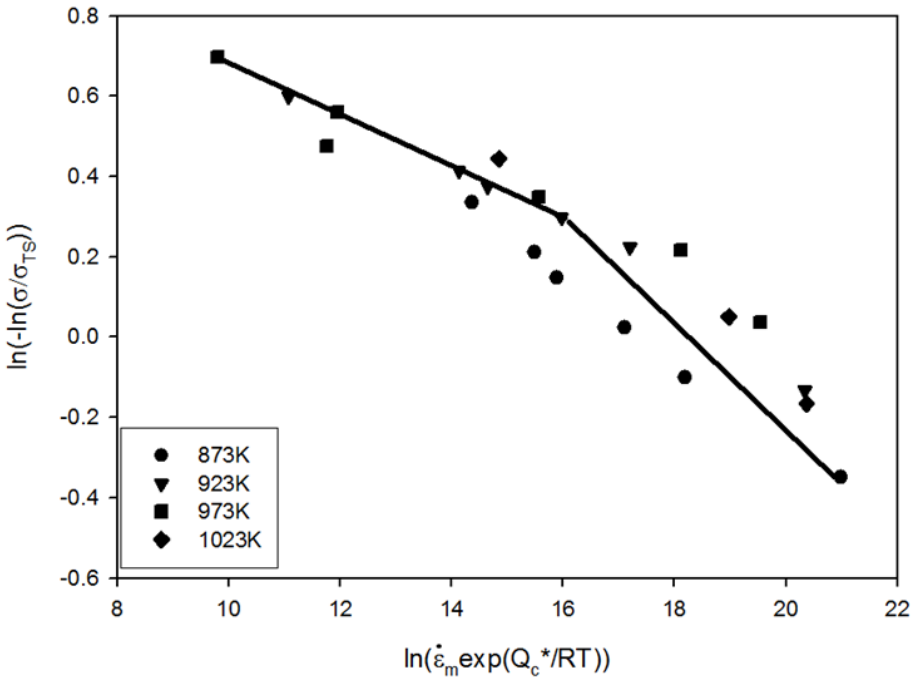

Figure 4. The variations of ln [$\dot{\varepsilon}_m$ exp (Q_c*/RT)] with ln[-ln (σ/σ_{TS})] for a sample of type 316 stainless steel tube, with Q_c*=250 kJmol^{-1} for $\sigma>\sigma_Y$ ($>\sigma_{PS}$) and Q_c*=150 kJmol^{-1} for $\sigma<\sigma_Y$ ($<\sigma_{PS}$).

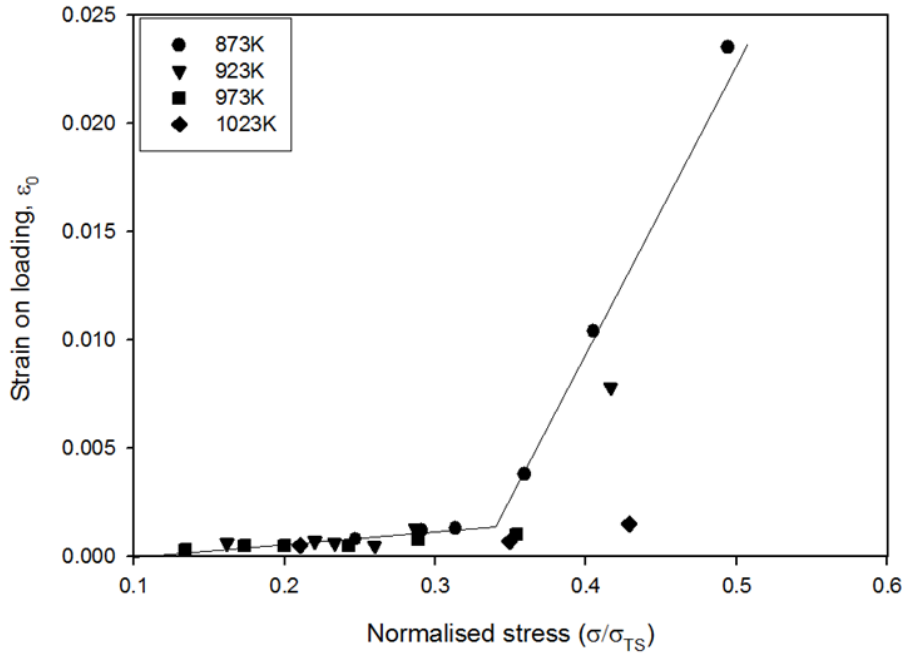

Figure 5. The variation of the initial strain on loading (ε_0) as a function of the normalized stress (σ/σ_{TS}) for type 316 stainless steel tube, showing only elastic ε_0 values when $\sigma<\sigma_Y<0.33\sigma_{TS}$ but with elastic and plastic ε_0 components when $\sigma>\sigma_Y>0.33\sigma_{TS}$.

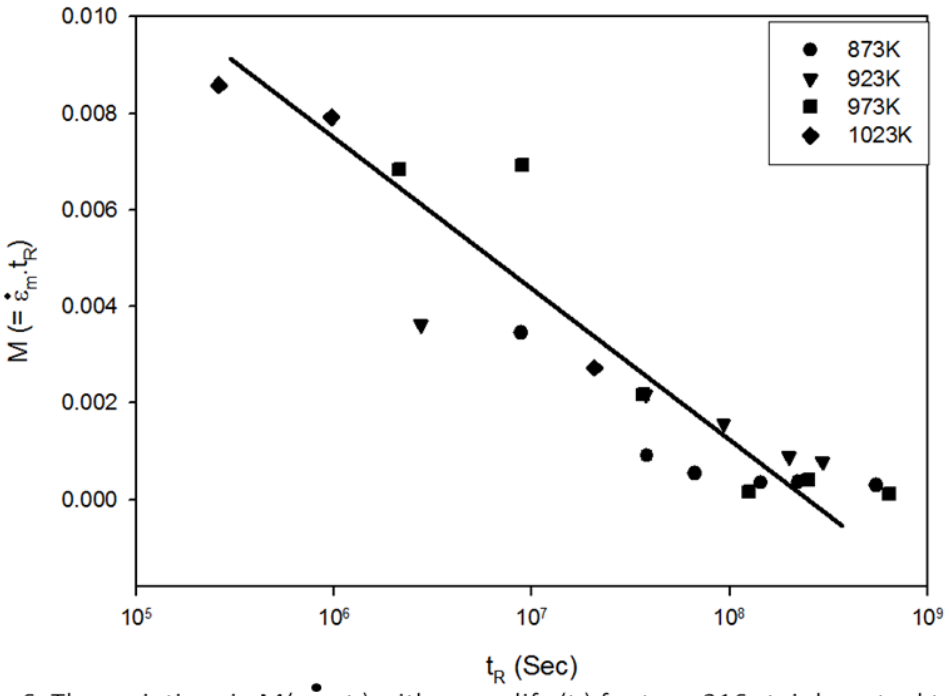

Figure 6. The variations in M(=$\dot{\varepsilon}_m t_f$) with creep life (t_f) for type 316 stainless steel tube, with M increasing from less than 0.001 to almost 0.01 as the creep life increases from $3.6\text{x}10^5$s to $3.6\text{x}10^8$s.

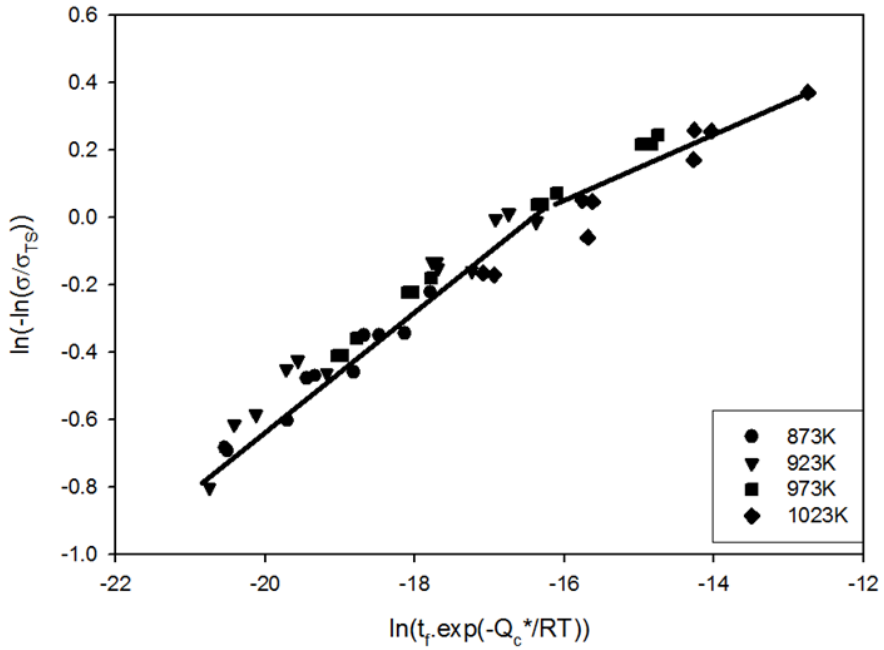

Figure 7. The variations of ln $[t_f \exp(-Q_c^*/RT)]$ with $[-\ln(\sigma/\sigma_{TS})]$ for a sample of type 316 stainless steel tube, with Q_c^*=250 kJmol^{-1} for $\sigma>\sigma_Y$ ($>\sigma_{PS}$) and Q_c^*=150 kJmol^{-1} for $\sigma<\sigma_Y$ ($<\sigma_{PS}$).

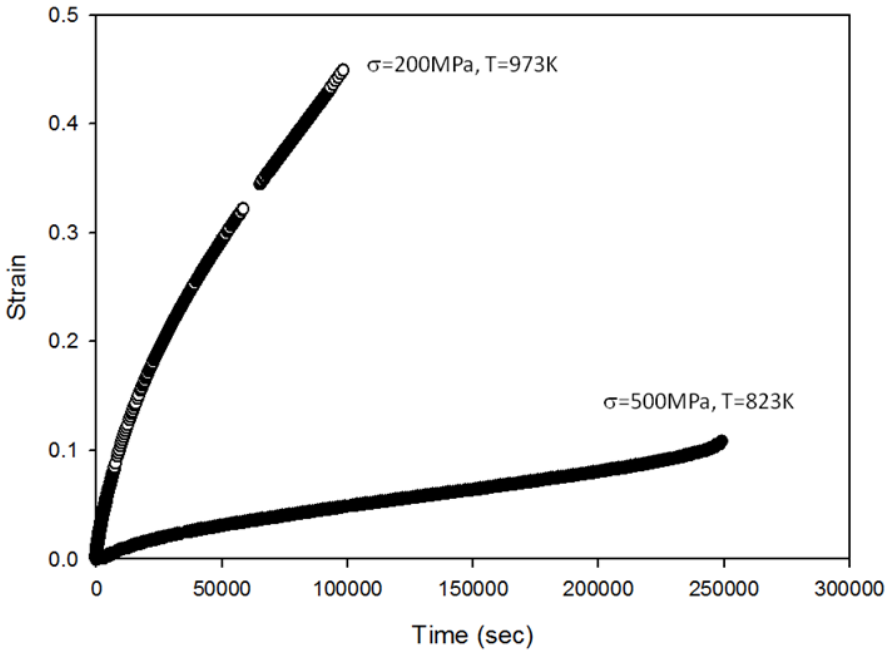

Figure 8. Normal creep strain (ε) against time (t) curves for type 316H stainless steel [13].

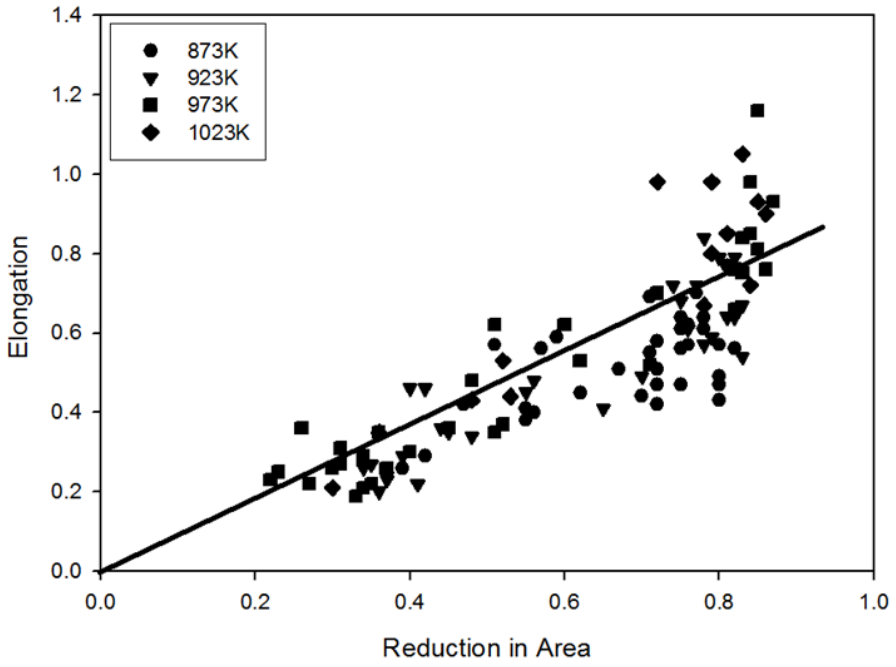

Figure 9. The broad relationship between the elongation at failure (ε_f) and the reduction in area at fracture (RoA) for type 316H stainless steel tube at 873 to 1023K.

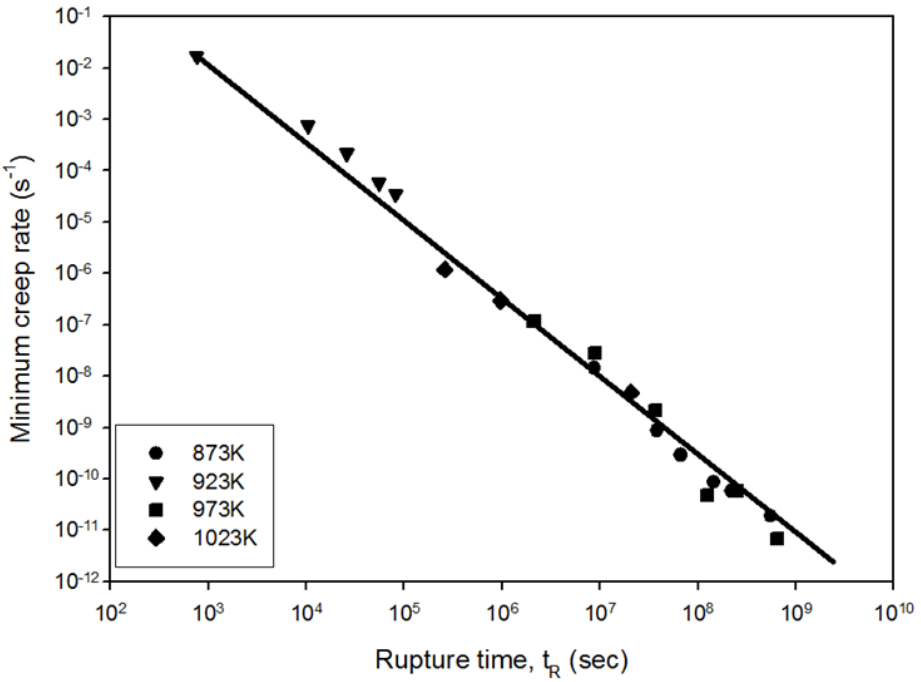

Figure 10. The dependence of the creep life (t_f) on the minimum creep rate ($\dot{\varepsilon}_m$) for type 316H stainless steel tube at 873 to 1023K.

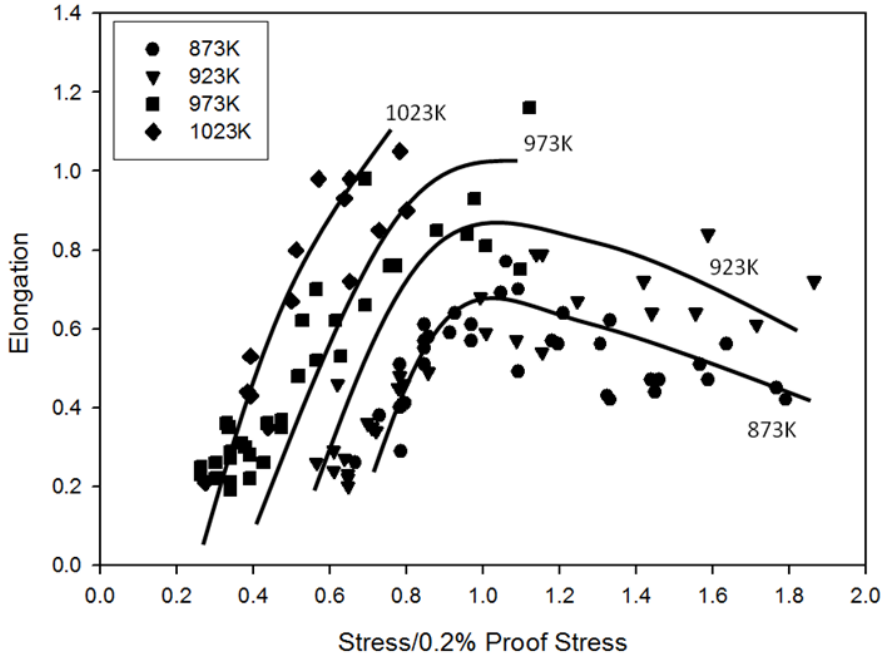

Figure 11. The dependence of the elongation at fracture (ε_f) on the normalized stress (σ/σ_{PS}), showing that ε_f falls sharply as the stress falls below σ_{PS} for type 316H stainless steel tube at 873 to 1023K.